LETTER *Special Section on Electronic Displays*

Defect Detection of TFT-LCD Image Using Adapted Contrast Sensitivity Function and Wavelet Transform*

Jong-Hwan OH[†], **Woo-Seob KIM**[†], ***Nonmembers***, **Chan-Ho HAN**[†], ***Member***, ***and*** **Kil-Houm PARK**[†a)], ***Nonmember***

SUMMARY The thin film transistor liquid crystal display (TFT-LCD) image has nonuniform brightness, which is a major difficulty in finding the Mura defect region. To facilitate Mura segmentation, globally widely varying background signal must be flattened and then Mura signal must be enhanced. In this paper, Mura signal enhancement and background-signal-flattening methods using wavelet coefficient processing are proposed. The wavelet approximation coefficients are used for background-signal flattening, while wavelet detail coefficients are employed to magnify the Mura signal on the basis of an adapted contrast sensitivity function (CSF). Then, for the enhanced image, trimodal thresholding segmentation technique and a false-region elimination method based on the human visual system (HVS) are employed for reliable Mura segmentation. The experimental results show that the proposed algorithms produce promising results and can be applied to automated inspection systems for finding Muras in a TFT-LCD image.

key words: *TFT-LCD, inspection, wavelet transform, human visual system, contrast sensitivity function*

1. Introduction

In flat-panel display (FPD) devices, thin-film-transistor liquid crystal displays (TFT-LCDs) outnumber other display devices in their volume and versatility of usage [1]. As the TFT-LCD market grows, the need for automated inspection systems increases. However, most of the final inspections of LCD panels have been carried out by human observers. Human-vision-based inspection systems have the disadvantage that each observer tends to have subjective defect decision levels, which can vary with time and physical conditions. Therefore, to increase the productivity and reliability of products, automated inspection systems are strongly required. TFT-LCD panel images suffer from nonuniform illumination factors such as the imperfection of the light source and the nonuniform liquid crystal distribution. Since TFT-LCD panels do not have a light source, they require an external light source known as a backlight unit (BLU). Despite every effort to make the BLU an ideal plane-light source, giving the entire TFT-LCD panel uniform brightness, BLU still produces illumination variations, measured by luminance uniformity (LU), of more than 80% [2]. LU is expressed as

$$luminance \quad uniformity \quad (LU) = \frac{L_{min}}{L_{max}} \times 100. \qquad (1)$$

where L_{max} and L_{min} are the maximum and minimum luminance values at predefined positions of a TFT-LCD panel, respectively. Generally, TFT-LCD signals are composed of a slowly varying background signal, a random noise signal and a defect or Mura signal [3] as shown in Fig. 1. In searching for the Muras in the observed (Seen) signal, the background signal is the main obstacle, although the noise signal, can't be neglected. Hence, to help separates the Muras, we must flatten the background signal, reduce the random noise and enlarge the Mura signal. The most effective and useful approach to facilitating Mura segmentation is background-signal flattening using polynomial approximation (PA) [4] or B-splines [5]. PA or B-splines seek the best-fitting surface or the plane that best describes the shape of the signal at a minimum mean-square-error point. However, PA or B-splines have a tendency to slightly reduce the difference between the background signal and the Mura signal. This makes it difficult to find Muras because they become fainter. Another approach to easy Mura segmentation is random-noise reduction. A denoising method, such as, the use of a wavelet transform (WT) has the best result in the case of precise noise modeling ([6], [7]). There is a problem in random-noise modeling because the TFT-LCD random noise signal is affected by the camera noise and the camera distortion and so on. And the other method of enabling Mura segmentation is the enhancement of the Mura signal. If the frequency band of the Mura signal could be found accurately, we could emphasize it by magnifying this band. Generally, the signal affects the entire frequency spectrum so that finding the precise cutoff frequency of the Mura signal is impossible. From a HVS point of view, we can emphasize more

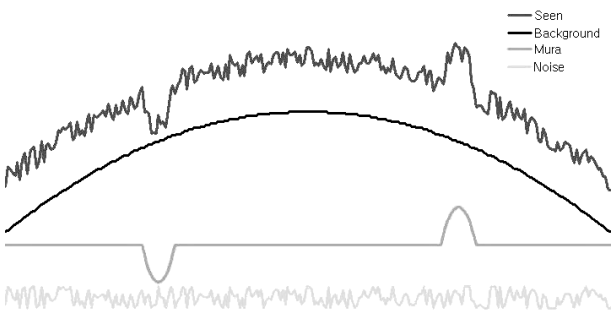

Fig. 1 Line profiles of TFT-LCD image.

Manuscript received February 28, 2007.
Manuscript revised May 10, 2007.

[†]The authors are with the School of Electrical Engineering and Computer Science, Kyungpook National University, 1370, Sankyuk-dong, Buk-gu, Daegu 702-701, Korea.

*This work was supported by grant No. (R01-2006-000-10944-0) from the Basic Research Program of the Korea Science & Engineering Foundation.

a) E-mail: khpark@ee.knu.ac.kr

DOI: 10.1093/ietele/e90–c.11.2131

visible frequencies, as demonstrated in the contrast sensitivity function (CSF) experiment [8]–[10]. In this paper, a TFT-LCD image defect detection algorithm using WT HVS is proposed. The main issue in wavelet domain signal processing is how to modify approximation coefficients (ACs) and detail coefficients (DCs) to values suitable for their applications. ACs are used for background-signal flattening purpose and DCs are utilized for Mura signal enhancement in this study. Then, trimodal thresholding, by which defect candidate are determined using statistical information, is employed for Mura segmentation. Finally, false-positive defects are reliably eliminated by Weber's law. The remainder of this paper is organized as follows. In the next section, the WT and CSF are simply introduced. Then the proposed TFT-LCD image defect detection algorithm is presented. Next, various experimental results are given. Finally, this paper is summarized with concluding remarks.

2. Wavelet Transform and Contrast Sensitivity Function

2.1 Wavelet Transform

Haar [11] found that a continuous signal can be expressed as the weighted sum of a wavelet basis. Since then, the WT has been used in various fields such as signal processing, function estimation, data compression, boundary extraction and denoising [6], [7]. The signal z can be expressed as the sum of two dilated and shifted orthogonal wavelet bases of scaling and wavelet functions:

$$z = \sum_k u_{j_0,k}\varphi_{j_0,k} + \sum_{j=j_0}^{\infty}\sum_k w_{j,k}\psi_{j,k}, \tag{2}$$

where $j,k \in Z, u_{j,k} = \int z(t)\varphi^*_{j,k}(t)dt$ and $w_{j,k} = \int z(t)\psi^*_{j,k}(t)dt$.

The dilated and shifted scaling wavelet bases are given as

$$\varphi_{j,k} = 2^{j/2}\varphi(2^j t - k), \psi_{j,k}(t) = 2^{j/2}\psi(2^j t - k), \tag{3}$$

For the image, the two-dimensional wavelet analysis and synthesis processes are given in Fig. 2. In the analysis stage at level j, the signal is low- or high-pass filtered horizontally, and downsampled vertically. Then the filtered signal is low- and high- pass filtered vertically, and downsampled horizontally. The low-pass-filter signal $W_\varphi(j,m,n)$ gives the ACs and $W^H_\psi(j,m,n), W^V_\psi(j,m,n,W), W^D_\psi(j,m,n))$ gives the DCs $j = 1$. The synthesis stage, the inverse process of the analysis stage, is also shown in Fig. 2(b). An example of the level 1 WT result of a test image is shown in Fig. 3.

2.2 Contrast Sensitivity Function

The HVS has different frequency sensitivity, which is mathematically represented as a CSF based on previous experimental results [8]–[10]. The HVS can more easily detect the

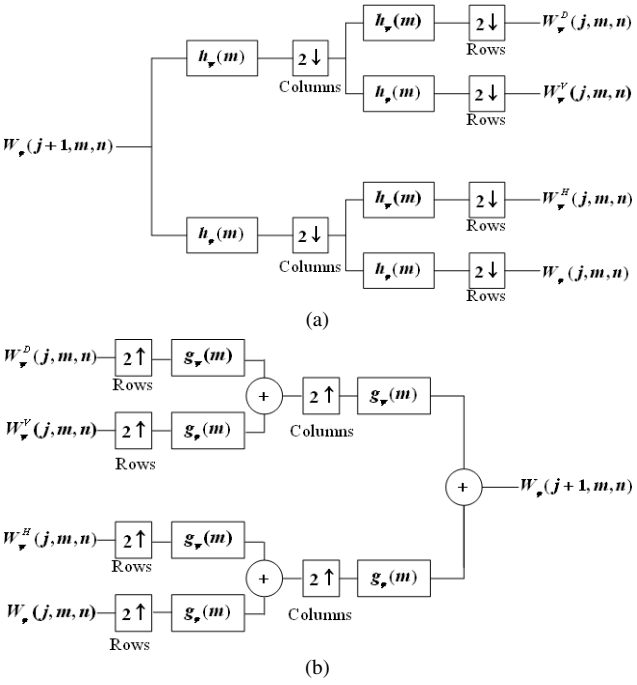

Fig. 2 2-D wavelet analysis and synthesis: (a) analysis, (b) synthesis.

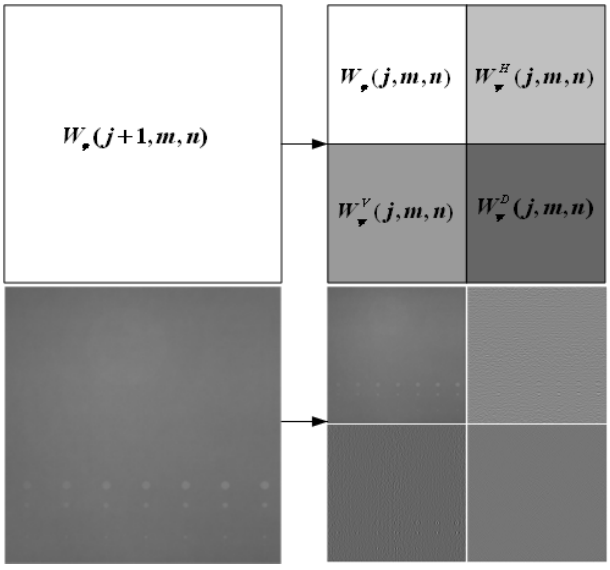

Fig. 3 Example image of wavelet analysis.

difference variation at low frequency than at high frequency. The CSF ($H(f)$) can be expressed as

$$H(f) = 2.6(0.192 + 0.114f)e^{-(0.114f)^{1.1}}, \tag{4}$$

where f is the frequency, having a unit of cycle/degree. The CSF graph is shown in Fig. 4. The HVS is most sensitive at around 8 [cycles/degree]. Above 40 [cycles/degree], its value becomes negligible. Previously, to use the CSF in image compression, for example, normalized spatial frequency is needed. The relative CSF value has a significant meaning. Without loss of generality, the CSF frequency can be normalized as $0 \sim \pi$.

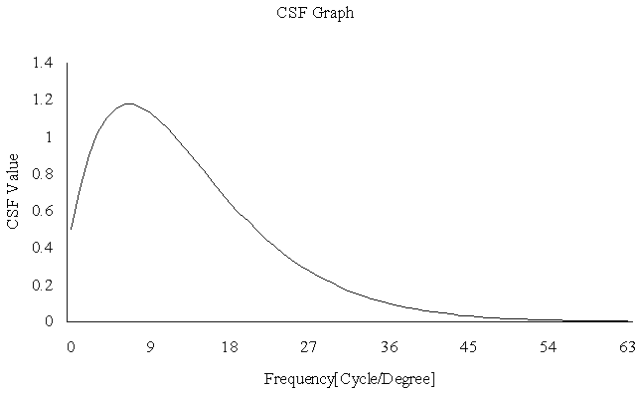

Fig. 4 Contrast sensitivity function graph.

3. Proposed Defect Detection Algorithm

The proposed defect detection algorithm is shown in Fig. 5. The input image undergoes a WT on the basis of defect size. The wavelet level is defined as 5 level if the defect size is less then 16×16 pixels, for example. The wavelet-transformed ACs and DCs are processed for different purposes. The ACs are used for flattening and DCs are used for defect signal enlargement. To maximize the flattening effect and to avoid affecting the shape significantly we replace the ACs with their mean value, and the DCs are weighted by the band-averaged value of the adapted CSF. Then, the transformed wavelet coefficients are synthesized. Next, the enhanced image is segmented by trimodal thresholding motivated by the fact that the gray level of defect pixels is brighter or darker than the surrounding pixels. To leave in reliable defect, false defects are eliminated if the defect mean gray level had small difference with the background gray level.

3.1 Wavelet Coefficient Processing

The WT signal processing deals precisely with the ACs and DCs. The wavelet-transformed ACs represent the low-pass-filtered signal and the DCs represent the high-pass-filtered signal. The ACs are used for signal flattening and the DCs are used for signal enlargement in this study. The ACs are replaced by the function $W^T_{AC}(X, Y)$ as follows:

$$W^T_{AC}(X, Y) = \frac{\sum_{x=1}^{M} \sum_{y=1}^{N} f_{ac}(x, y)}{M \times N}, \tag{5}$$

where $f_{ac}(x, y)$ represents the wavelet-transformed ACs and M and N are heights and widths, respectively. The DCs are weighted by the band-averaged value of the adapted CSF $W^W_{DC}(X, Y)$ as

$$W^T_{DC}(X, Y) = W^W_{DC}(x, y) \times f_{dc}(x, y), \tag{6}$$

where $W^T_{DC}(X, Y)$ are the transformed DC coefficients, and $W^W_{DC}(X, Y)$ and $f_{dc}(x, y)$ are the band averages of the adapted CSF and the original DC coefficients within the subband, repectively. The $W^W_{DC}(X, Y)$ are given as

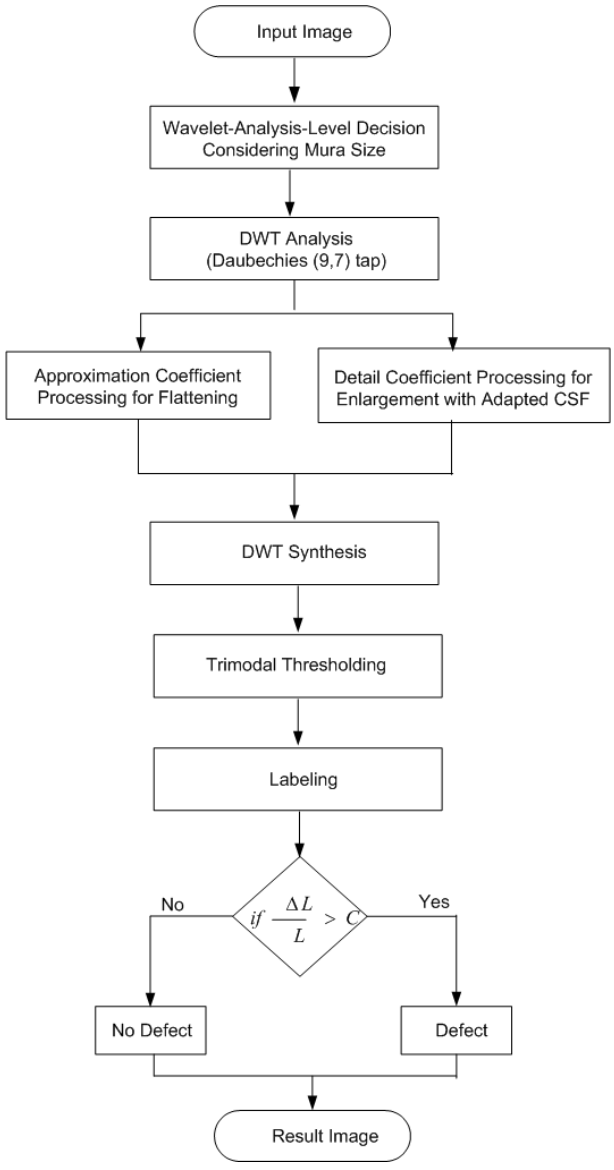

Fig. 5 Block diagram of proposed TFT-LCD image defect detection.

$$W^W_{DC}(X, Y) = \frac{\int_{B_l} ACSF(f_{nor})}{\int_{B_l} dw}, B_l = \left(\frac{\pi}{2^l}, \frac{\pi}{2^{l-1}}\right), \tag{7}$$

where B_l are the wavelet subbands for wavelet analysis level l. The adapted CSF is expressed as

$$ACSF(f_{Nor}) = \frac{H(f/64 \times \pi)}{H(0)}, \tag{8}$$

where $H(0)$ is a constant value of 0.4992 and the ACSF and wavelet mask values $W^W_{DC}(X, Y)$ are shown in Fig. 6.

3.2 Trimodal Thresholding

After the TFT-LCD image is enhanced in the wavelet domain, the defects are segmented by trimodal thresholding [3] to find brighter and darker Muras simultaneously. The trimodal thresholding function $f_T(x, y)$ is given as

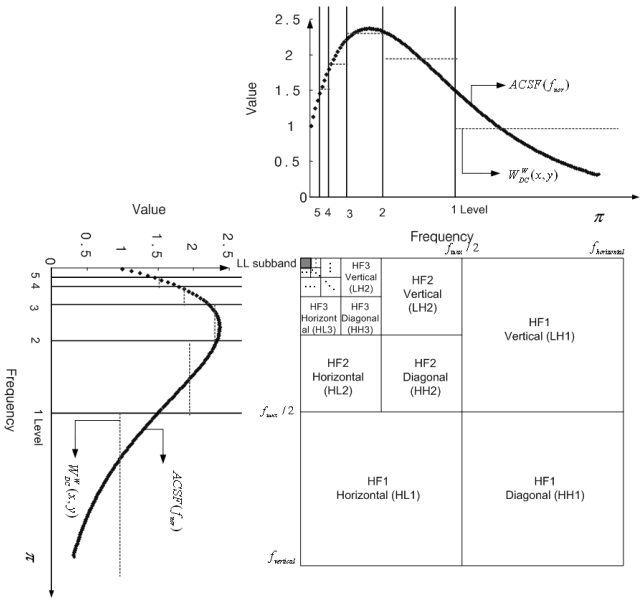

Fig. 6 ACSF and wavelet mask values in WT domain.

$$f_T(x,y) = \begin{cases} 255 & \text{if } (f(x,y) > m + k\sigma) \\ 128 & \text{elseif } (f(x,y) < m + k\sigma) \\ 0 & \text{else,} \end{cases} \tag{9}$$

where $f(x,y)$ is the gray level at position (x,y), and m and σ are the mean and standard deviation, respectively. k is a constant used to determine the amount of abnormal gray level. After trimodal thresholding, the bright and bark Muras have values of 255 and 128, respectively, and the background region has a value of 0.

3.3 Defect Analysis

The segmented result may include false defects such as noise and neglected small regions. Thus, for reliable defect confirmation, defect analysis processing is needed. In this paper, a HVS-based false-region elimination method is proposed. The noticeable luminance difference is given by the Weber constant, C_{Weber}, in the Weber region as follows [12]:

$$C_{Weber} = \frac{\Delta L}{L}, \tag{10}$$

where L and ΔL are the background-region luminance and the luminance difference between the background region and the defect region, respectively. We use a C_{Weber} value of 0.02 in this study.

4. Experimental Results

The proposed method is tested using 40 real Muras and 60 generated ones. Very faint defects are also added in our experiment. The acquired TFT-LCD images have 400 μm spatial resolution for each pixel and 8-bit brightness resolution. To evaluate the performance of the proposed algorithm, 1-D line profiles, 2-D enhanced images and the final segmented

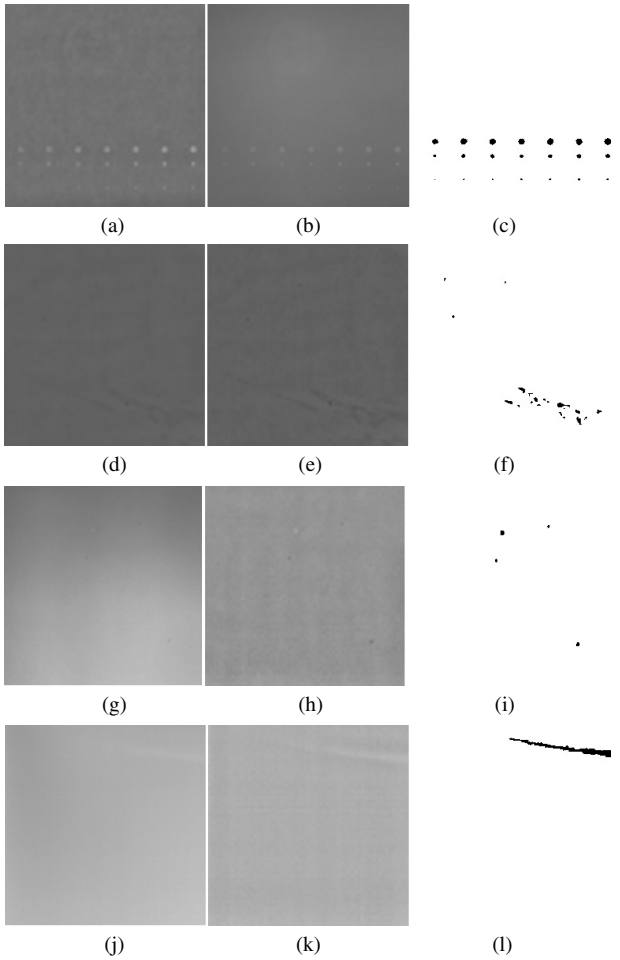

Fig. 7 Results of proposed method. (a), (d), (g) and (j) are test images; (b), (e), (h) and (k) are enhanced images; and (c), (f), (i) and (l) are the final segmented results of the original images (a), (d), (g) and (j), respectively.

Muras are shown along with a detection accuracy table. In our experiment, the Daubechies (9,7) tap wavelet is used. The wavelet analysis level is determined to be 5 by considering the size of the Muras. The results of the proposed defect detection method are shown in Fig. 7. The test image in Fig. 7(a) has artificially generated Muras with various strengths and sizes. In the enhanced image Fig. 7(b), the defects are more visible than in the original image, which is also more evident in Figs. 7(e), (h), and (k). The original image in Fig. 7(g) has considerable background variation, so the defects are difficult to see in the original image. However, the enhanced image has a relatively flattened background and the defects are more visible. In the test image in Fig. 7(j), we obtain novel enhancement that induces a clear final segmentation.

The results of microscopic enhancement results using the line profiles are shown in Fig. 8. Figures 8(a), (b) and (c) show the results for corresponding the enhanced profiles to Figs. 7.(b), (e) and (h). In these results, the effectiveness of our algorithm is shown more clearly. In the filtered line profile results, denoted by WT64, we can clearly observe that the proposed enhancement method can flatten

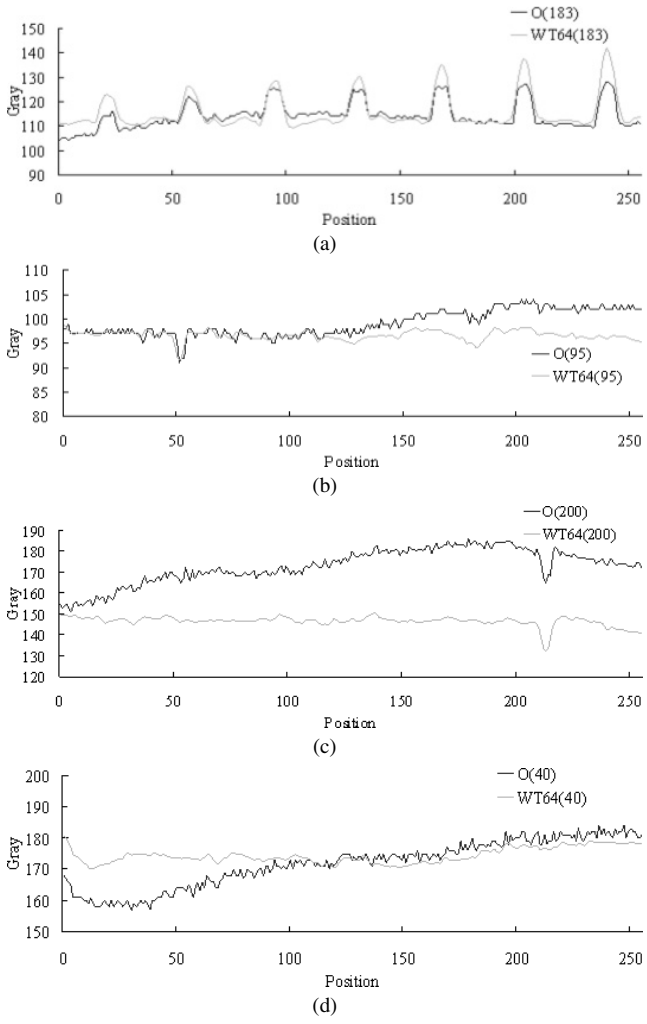

Fig. 8 Line profiles of the proposed method. (a), (b), (c) and (d) are original and proposed line profiles corresponding to Figs. 7(a), (d), (g), and (j), respectively.

Table 1 Experimental results for the detection of Muras.

# of Defects	False-positive rate	False-negative rate
100	0.04	0.02

the background-signal fluctuation and enlarge the defect region. The results for a faint scratch line profile are shown in Fig. 8(d). The scratch exists at line 40 of the original 256×256 image. Compared with the original line profile (O(40)), the line profile of the enhanced image has a significantly increased gray level. From the experimental results, it is confirmed that the proposed method strongly enhances the TFT-LCD image.

Finally, the performance results are summarized in Table 1. The false-positive and false-negative measures are used to evaluate the accuracy of defect detection. There are some problems regarding the elimination of defects existing at the boundary region and very weak small defects. Except for such cases, the false-positive rate and false-negative rate are acceptable.

5. Conclusions

In this study, a new defect detection algorithm for TFT-LCD images that produces enhanced images by WT domain processing was developed. The wavelet-transformed ACs and DCs were used for different purposes. The wavelet ACs were used for flattening by replacing the ACs with their mean value, while the DCs were used to enlarge the defect region using the adapted CSF. Then a trimodal thresholding segmentation method was employed to find bright Muras and dark Muras at the same time. Finally, reliable defect confirmation based on Weber's constant was used for eliminating falsely detected defects. The effectiveness of our algorithm was tested by considering two factors: image enhancement and final segmentation result. In macro-enhanced images and microline profiles, background flattening and Mura signal enlargement were clearly seen. The final defect detection results were also evaluated. The experimental results indicated that the proposed method produces promising results for finding defects in TFT-LCD images and can be applied to similar FPD images.

References

[1] J. Jang, S.K. Lim, and M.H. Oh, "Technology development and production of flat panel displays in Korea," Proc. IEEE, vol.90, no.4, pp.501–513, 2002.
[2] VESA Flat Panel Display Measurements Standard Ver 2.0, June 1, 2001.
[3] J.H. Oh, D.M. Kwak, K.B. Lee, Y.C. Song, D.H. Choi, and K.H. Park, "Line defect detection in TFT-LCD using directional filter bank and adaptive multilevel thresholding," Key Engineering Materials, vol.270-273, pp.233–238, 2004.
[4] S.I. Baek, W.S. Kim, T.M. Koo, I. Choi, and K.H. Park, "Inspection of defect on LCD panel using polynomial approximation," TENCON 2004, vol.A 21-24, pp.235–238, Nov. 2004.
[5] G.B. Lee, C.G. Lee, S.Y. Kim, and K.H. Park, "Adative surface fitting for inspection of FPD devices using multilevel B-spline approximation," 21st International Technical Conference on Circuits/Systems, Computers and Communications, vol.2, pp.205–208, 2006.
[6] D.L. Donoho and I.M. Johnstone, "Adapting to unknown smoothness via wavelet shrinkage," J. American Statistical Association, vol.90, no.432, pp.1200–1225, Dec. 1995.
[7] I.K. Fodor and C. Kamath, "Denoising through wavelet shrinkage: An empirical study," J. Electronic Imaging, vol.12, pp.151–160, 2003.
[8] X. Liang and H. Wu, "Multiple perceptual watermarks using multiple-based number conversion in wavelet domain," Proc. ICCT2003, pp.213–216, 2003.
[9] A. Gaddipatti, R. Maciraju, and R. Yagel, "Steering image generation with wavelet based perceptual metric," Comput. Graph. Forum, vol.16, no.3, pp.C241–C251, Sept. 1997.
[10] G.M. Johnson and M.D. Fairchild, "On contrast sensitivity in an image difference model," PICS2002, pp.18–23, April 2002.
[11] A. Haar, "Zur Theorie der orthogonalen Funktionensysteme," Mathematische Annalen, vol.69, pp.331–371, 1910.
[12] S. Hecht, "The visual discrimination of intensity and the Weber-Fechner law," J. General Physiology, vol.7, pp.235–267, Sept. 1924.